Macromolecules
ARTICLE

Macromolecules **2009**, *42*, 8827–8834 **8827**
DOI: 10.1021/ma9018729

Locally Anisotropic Porous Materials from Polyethylene and Crystallizable Diluents

Joonsung Yoon, Alan J. Lesser,* and Thomas J. McCarthy*

Polymer Science and Engineering Department, University of Massachusetts, Amherst, Massachusetts 01003

Received August 22, 2009; Revised Manuscript Received October 3, 2009

ABSTRACT: Locally anisotropic porous materials were prepared using linear low-density polyethylene (LLDPE) and crystallizable organic diluents by thermally induced phase separation processes. Pyrene and hexamethylbenzene (HMB) were selected as crystallizable diluents because of their miscibility with LLDPE at elevated temperature, higher crystallization temperatures than that of LLDPE, and their individual (very different) crystallization behaviors. Equilibrium phase diagrams were calculated using the Flory−Huggins theory of solution thermodynamics and show good agreement with experimental observations. The phase separation process, which was monitored visually using an optical microscope equipped with a temperature controller, shows strong dependence on solution composition as well as the diluent identity. Solidified materials after extraction of pyrene from pyrene/LLDPE mixtures exhibit locally aligned layers of pores, with features that depend on solution composition. The pores inside semicrystalline polyethylene domains are aligned in the crystal growth direction of pyrene, which crystallizes before LLDPE upon cooling. When HMB is the crystallizable diluent, platelike pore structures, much larger in size than the pyrene-derived pores, are observed, consistent with reports of other investigators. These observations are discussed in terms of the phase transformation processes caused by the different crystallization behavior of the diluents.

Introduction

Thermally induced phase separation (TIPS) processes are widely used to prepare microporous polymeric membranes due to their simplicity and ability to control phase separation.[1,2] Typical TIPS processes proceed either by liquid−liquid phase separation, resulting in a polymer-rich continuous phase and a polymer-lean droplet phase, or by liquid−solid (L−S) phase separation, in which the polymer solidifies from solution.[2] Systems exhibiting an upper critical solution temperature (UCST), in which a homogeneous mixture of a polymer with a diluent at an elevated temperature does not form a single phase at a lower temperature, are often used.[3] In these cases, the homogeneous polymer solution undergoes L−L phase separation upon cooling. The droplet phase, composed of nearly pure diluent, is uniformly dispersed in the polymer-rich matrix phase and can be removed from the solidified mixture to yield a cellular structured microporous membrane. Since the droplet phase determines the cellular structure of the porous membrane, the cellular morphology of the membrane can be controlled by changing temperature profiles and using a variety of combinations of polymers and diluents. While there is a significant literature regarding this control,[1−5] relatively little effort has been expended to control the shape of the pores. Narkis et al. observed three modes of crystallization (needlelike, dendritic, and tiny crystalline particles) when low molecular weight organic compounds were used in amorphous polymers.[6] Smith et al. reported a rodlike eutectic microstructure from the quasi-binary system of unfractionated isotactic polypropylene and the dendritic growing diluent, pentaerythrityl tetrabromide.[7] This group also reported cleaved, truncated HMB needles grown in a polyethylene matrix.[8] Alwattari et al. used isotactic polypropylene blended with HMB to investigate the effects of melt composition and crystallization temperature on the microstructure of the resulting membranes, which were composed of rectangular pores with secondary needlelike structures.[9] It is not, however, clear how different high melting, crystallizable diluents lead to different morphologies or how this process might be used to control structure in porous materials.

Here we describe research aimed at the preparation of porous polymeric materials with controlled pore shape and size using linear low-density polyethylene (LLDPE) in combination with the high melting diluents, pyrene and hexamethylbenzene (HMB). Different morphologies of the resulting porous structures were investigated and are discussed in terms of phase diagrams and crystallization behavior of each diluent in the polymer solutions. These studies suggest that crystallizable diluents may be useful for polymer structure control.

Experimental Section

Materials. Linear low-density polyethylene (Dowlex LLDPE-2553) was obtained from Dow. Pyrene (98% purity) and HMB (99% purity) were purchased from Fisher Scientific and used without further purification. The crystalline diluents were chosen because of their melting temperatures and structural similarity with known solvents for polyethylene (e.g., xylenes). Information concerning the crystallography of the diluents can be found in the literature.[10,11] The molecular weight of the polyethylene was determined by gel permeation chromatography (GPC, PL-GPC 220) at 145 °C using trichlorobenzene as the elution solvent. Thermal properties were determined by differential scanning calorimetry (DSC-2910, TA Instruments) at 5 °C/min heating and cooling rates. Other properties were obtained from referenced literature and are summarized in Table 1.

Sample Preparation. LLDPE powder was prepared by dissolution of the provided pellets in refluxing xylene, precipitation in excess methanol, and subsequent drying in a vacuum oven at 80 °C overnight. The powdered sample obtained was mechanically crushed to prepare free-flowing powders. Pyrene and

*Corresponding authors. E-mail: ajl@polysci.umass.edu (A.J.L.), tmccarthy@polysci.umass.edu (T.J.M.).

Published on Web 10/13/2009

Table 1. Materials Properties

properties	units	LLDPE	HMB	pyrene
molecular weight	g/mol	18 000 (M_n) 108 000 (M_w)	162	202
degree of polymerization		642	N/A	N/A
molar volume	cm^3/mol	33.03[a] (ethylene unit)	175[b]	179[c]
density	g/cm^3	0.935	0.926[b]	1.27
heat of fusion	J/mol	3780 (ethylene unit)	21 840	17 310
melting temperature	K (°C)	402 (129)	440 (167)	426 (153)
crystallization temperature	K (°C)	382 (109)	436 (163)	394 (121)
solubility parameter	$MPa^{1/2}$	17[d]	17[b]	20.7[c]

[a] Representative value (ref 12). [b] Representative value (ref 13). [c] Representative value (ref 14). [d] Representative value (refs 12 and 15).

HMB were crushed to make fine powders. Diluent powder samples were premixed with LLDPE powder in various compositions in a glass vial to yield a total weight of 1 ± 0.05 g. The vials were purged with nitrogen for 30 min, sealed (screw cap), and immersed in an oil bath at 200 °C for 10 h. Compositions prepared ranged from 10 to 90 wt % diluent at 5−10 wt % intervals. After completion of thermal mixing, samples were rapidly cooled by immersion in liquid nitrogen to prevent macroscopic phase separation. Quenched samples were chopped and weighed before being used to make plaque specimens with a compression molding machine (PW2256, PHI Co.). Each sample was weighed into a square mold (25 mm × 25 mm, 0.5 mm in thickness), melted at 200 °C for 3 min under 35 MPa pressure, and then cooled rapidly using a second compression molder (Carver laboratory press) which was maintained at 20 °C and operated under 35 MPa pressure. The composition of each sample after the compression molding was determined by thermal gravimetric analysis (TGA-2950, TA Instruments). Diluents were removed by overnight Soxhlet extraction using appropriate solvents (methanol for pyrene, acetone for HMB). After extraction, samples were dried in a vacuum oven at 60 °C overnight. The extraction efficiency was checked by TGA and found to be higher than 95% for all samples.

Thermal Analysis. Differential scanning calorimetry (DSC-2910, TA Instruments) was used to determine melting and crystallization temperatures. Each diluent−polymer mixture sample was hermetically sealed in an aluminum DSC pan, heated from 25 to 200 °C at 10 °C/min, and maintained at 200 °C for 3 min. Samples were then cooled to 50 at 5 °C/min to measure crystallization temperature. Samples were heated again to 200 at 5 °C/min to measure melting temperature. Peak maxima were taken as melting and crystallization temperatures.

Optical Microscopy. An Olympus BX51 microscope was used to visualize the phase separation process. A small section was sliced from each diluent−polymer mixture sample and placed between pairs of microscope slides. The edges of the slides were sealed with Teflon tape to prevent material loss by evaporation. A hot stage (Linkam TMS-93) with a temperature controller (Linkam THMS-600) was used to heat samples at 5 °C/min to 200 °C at which temperature they were maintained for 3 min and then cooled to 30 at 5 °C/min. The thermocouple for temperature measurement was located near the heating block of the hot stage, and the slide/sample assemblies were not insulated; thus, the actual temperature of the samples is lower than that recorded by the thermocouple. This issue was addressed by calibrating the temperature reading from the thermocouple using several organic molecules with sharp melting temperatures in the temperature range suitable for our experiments (naphthalene: 80.6 °C; phthalic anhydride: 130.8 °C; pyrene: 156 °C; hexamethylbenzene: 164 °C). Temperatures at which the sample suddenly became turbid and/or diluent crystals began to grow in the polymer-rich matrix were recorded.

Scanning Electron Microscopy (SEM). Morphology of the cross sections of the samples after removal of the diluents was examined by field emission scanning electron microscopy (JEOL FX-6210) with an accelerating voltage of 10 kV. Cross sections of the samples were prepared by immersion in liquid nitrogen (5 min) followed by fracture of the samples (sharp razor blade). The exposed cross section was coated with Au using a sputter coating instrument (Cressington sputter coater 108). SEM images were obtained from at least five different locations on each sample.

Results and Discussion

Equilibrium Phase Diagrams. Equilibrium phase diagrams were calculated for binary mixtures of pyrene/LLDPE and HMB/LLDPE based on Flory−Huggins solution thermodynamics. Details of the methods used can be found in the literature.[16−18] The theoretical melting temperature depression of LLDPE in which crystalline LLDPE is in equilibrium with a polymer solution is calculated using eq 1

$$\frac{1}{T_m} = \left[1+\frac{R\beta}{\Delta H_u}\left(\frac{V_u}{V_1}\right)(1-\phi_2)^2\right]^{-1} \left[\frac{1}{T_m^0}+\frac{R}{\Delta H_u}\left(\frac{V_u}{V_1}\right)\left\{\left(1-\frac{1}{N}\right)(1-\phi_2)-\frac{\ln(\phi_2)}{N}\right\}\right] \quad (1)$$

where T_m is the melting temperature of LLDPE in a polymer solution, T_m^0 is the melting temperature of neat LLDPE, ΔH_u is the enthalpy of fusion per repeat unit of LLDPE, N is the degree of polymerization, ϕ_2 is the volume fraction of LLDPE, R is the gas constant, and β is a constant which is calculated from the solubility parameters of LLDPE (δ_2) and diluent (δ_1) along with the molar volume of diluent (V_1), using the equation $(\delta_1 - \delta_2)^2 V_1/R$. Six ethylene units are considered as the repeat unit so that the molar volume of LLDPE repeat unit (V_u) and that of diluent (V_1) are similar, as assumed in Flory−Huggins theory. Thus, the values of the degree of polymerization (N), enthalpy of fusion (ΔH_u), and molar volume of LLDPE repeat unit (V_u) in eq 1 are adjusted by considering six ethylene units as a repeat unit. Similarly, the melting temperature depression of diluent in which the crystalline diluent is in equilibrium with the polymer solution is calculated using eq 2

$$\frac{1}{T_{m,1}} = \left[1+\frac{R\beta\phi_2^2}{\Delta H_1}\right]^{-1} \left[\frac{1}{T_{m,1}^0}-\frac{R}{\Delta H_1}\left\{\left(1-\frac{1}{N}\right)\phi_2+\ln(1-\phi_2)\right\}\right] \quad (2)$$

where $T_{m,1}$ is the melting temperature of crystalline diluent in a polymer solution, $T_{m,1}^0$ is the melting temperature of neat diluent, and ΔH_1 is the enthalpy of fusion for neat diluent. Experimental values of melting temperatures measured using DSC at a 5 °C/min heating rate show good agreement with calculated results as shown in Figures 1 and 2. Since the

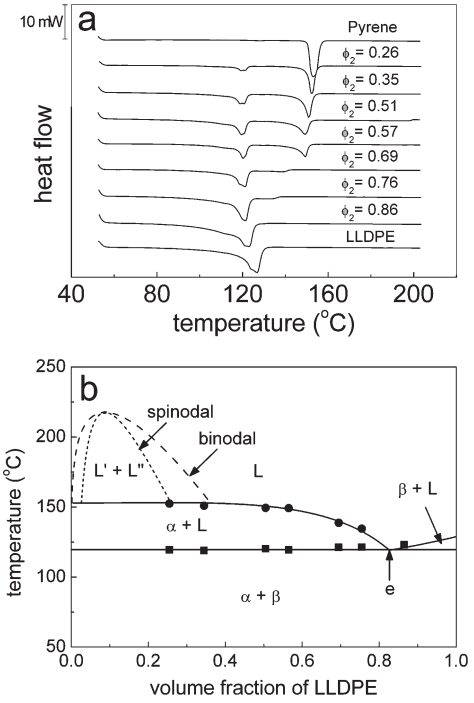

Figure 1. Thermal analysis results for mixtures of pyrene and LLDPE. (a) DSC thermograms of selected mixtures for melting temperature determination; heating rate was 5 °C/min; ϕ_2: volume fraction of LLDPE. (b) Melting temperature plotted on the calculated equilibrium phase diagram. Solid pyrene: β = solid LLDPE; L, L′, L″ = liquid mixture of pyrene and LLDPE; e = eutectic point. Note that L−L demixing (binodal, spinodal) is not confirmed under these experimental conditions.

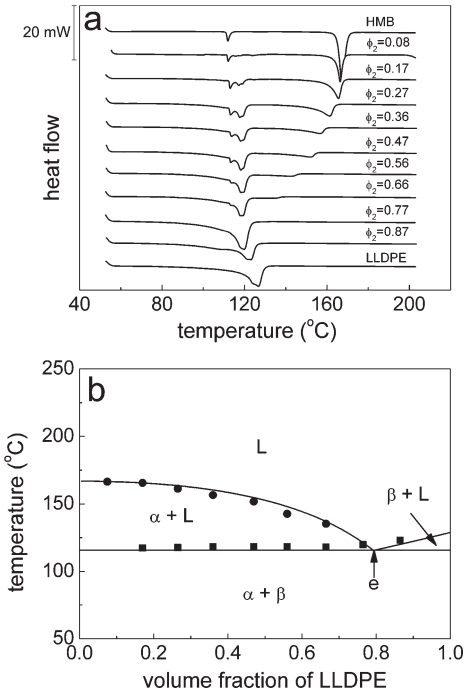

Figure 2. Thermal analysis results for mixtures of HMB and LLDPE. (a) DSC thermograms of selected mixtures for melting temperature determination; heating rate was 5 °C/min; ϕ_2: volume fraction of LLDPE. (b) Melting temperature plotted on the calculated equilibrium phase diagram. α = solid HMB; β = solid LLDPE; L, L′, L″ = liquid mixture of HMB and LLDPE; e = eutectic point.

melting temperature (T_m) depression as represented by the liquidus lines in Figures 1 and 2 is colligative property, T_m depression of the diluent depends on the "number" of

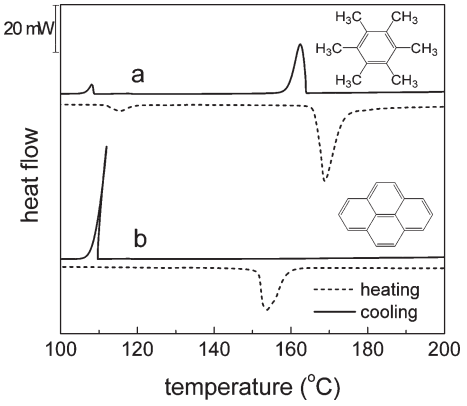

Figure 3. DSC melting (dashed lines) and crystallization (solid lines) thermograms of pure diluents at 5 °C/min heating and cooling rates. (a) HMB, small melting peak at around 120 °C and small crystallization peak at around 110 °C are assumed to be from impurities. (b) Pyrene.

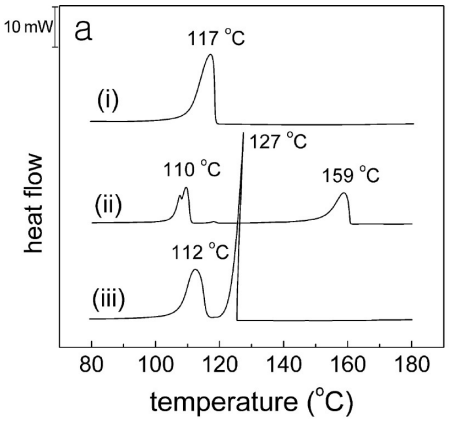

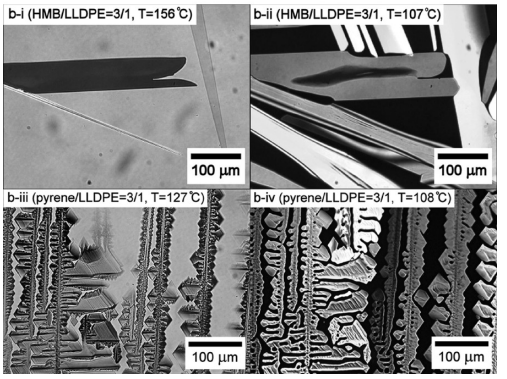

Figure 4. Crystallization process analysis for binary mixtures of LLDPE with HMB and pyrene. The volume fraction of LLDPE in the mixture was fixed at ϕ_2 = 0.25. (a) Crystallization peaks from DSC obtained at a cooling rate of 5 °C/min: (i) neat LLDPE, (ii) HMB/LLDPE, (iii) pyrene/LLDPE. (b) Micrographs from optical microscopy. Samples were cooled from 200 to 30 °C at 5 °C/min. (i) Crystallization of HMB begins at 156 °C for HMB/LLDPE, (ii) crystallization of HMB is complete at 107 °C for HMB/LLDPE (cross-polarized image), (iii) crystallization of pyrene begins at 127 °C for pyrene/LLDPE, and (iv) crystallization of pyrene is complete at 108 °C for pyrene/LLDPE (cross-polarized image).

molecules of the polymer and vice versa. Because of the large molecular weight of the polymer, the melting point of the diluent does not decrease sharply as the volume fraction of the polymer increases while that of the polymer decreases relatively sharply as the volume fraction of the diluent increases because of the small molecular weight of the diluent. As a result, the eutectic composition (marked "e"

in Figures 1 and 2) is located in the polymer-rich regime. The resulting equilibrium phase diagrams suggest that phase separation is most likely induced by the crystallization of the diluent rather than that of the polymer, unless the initial composition is highly polymer-rich.

If the polymer content in the initial mixture is lower than the eutectic composition, phase separation is initiated by the crystallization of the diluent upon cooling. The diluent will begin to crystallize and will be precipitated from the polymer solution when the temperature reaches the melting temperature of the diluent at that composition (this assumes idealized equilibrium crystallization conditions). Upon further cooling, more crystals of diluent will be formed from the liquid solution, causing the polymer content in the liquid solution to increase until it reaches the eutectic composition. Both the polymer and diluent crystallize at the same time when the composition of the liquid solution reaches the eutectic composition. Eutectic transformation ($L \rightarrow \alpha + \beta$) occurs at a constant temperature, shown as eutectic horizontal lines in Figures 1b and 2b, because of the zero degrees of freedom at that condition.[18] Gibb's phase rule at fixed pressure states that $F = C - P + 1$ (F: degrees of freedom; C: number of components; P: number of phases) and $F = 0$ at eutectic conditions since there are two components ($C = 2$) and three phases (L, α, β) coexisting ($P = 3$), making the temperature invariant. It should also be noted that solid solubility (solubility of solid solute in solid solvent) is assumed to be negligible in Figures 1b and 2b because of the significant difference in crystal structure and size between the polymer and each diluent; crystals of each component are assumed to be pure, which is often the case for organic binary mixtures.[19]

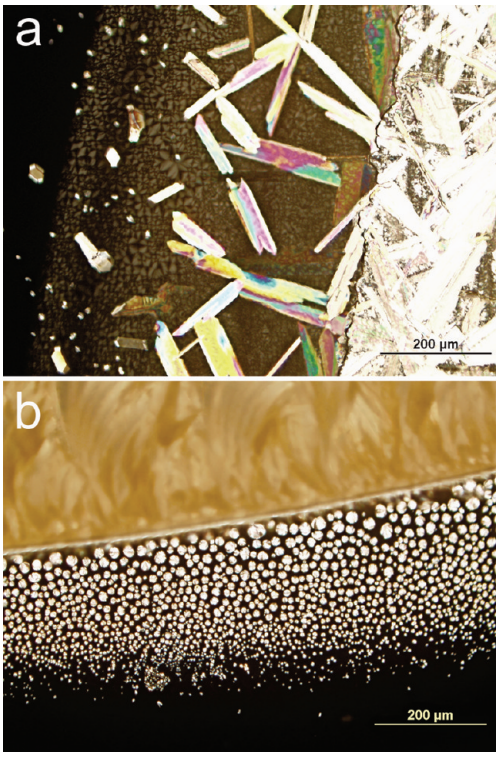

Figure 5. Polarized optical microphotographs of the solid−liquid interface. Thin (~10 μm) samples of diluent/polymer (3/1, w/w) mixtures were quickly quenched from 200 to 20 °C. (a) HMB/LLDPE, (b) pyrene/LLDPE.

Because of the poor solvent quality of pyrene for LLDPE, mixing becomes difficult as the pyrene content increases. Since the χ parameter is a function of temperature and solvent quality improves as temperature increases for these mixtures, thermal mixing was carried out at as high as 200 °C. The mixing temperature is limited by the thermal stability of pyrene; at temperatures higher than 200 °C, severe discolorization of pyrene is observed. The highest possible content of pyrene in the mixture is about 75 vol %; homogeneous mixtures of greater pyrene concentration cannot be formed at 200 °C. Since the calculated phase diagram predicts L−L demixing at 200 °C if the volume fraction of pyrene is greater than ca. 0.8, incomplete mixing at this composition regime is most likely due to L−L demixing. However, L−L demixing (Figure 1b) could not be confirmed experimentally due to the thermal instability of pyrene. In contrast, mixing is straightforward for HMB and LLDPE due to their good miscibility and similar densities in the liquid state. Since the solubility parameters of LLDPE and

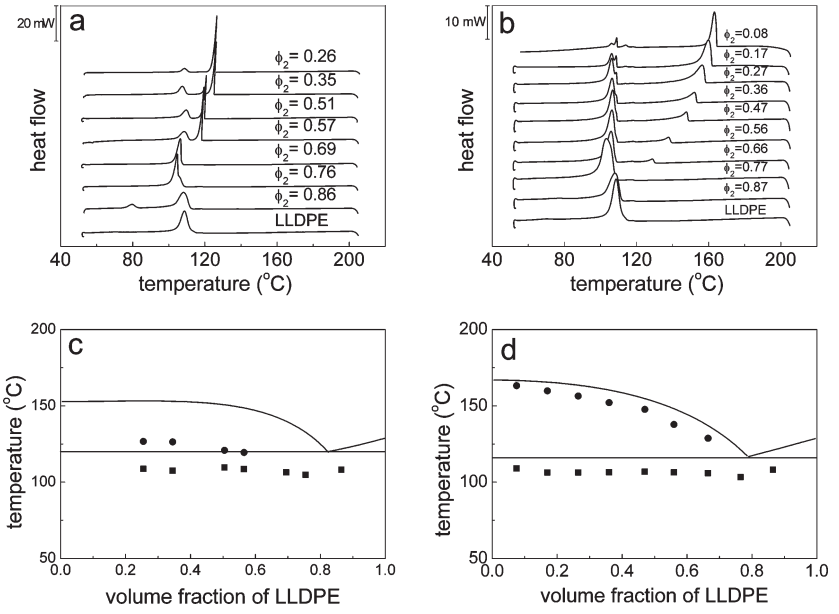

Figure 6. Crystallization temperatures determined by DSC cooling runs at 5 °C/min; ϕ_2 = volume fraction of LLDPE. (a) Pyrene and LLDPE mixtures. (b) HMB and LLDPE mixtures. (c) Crystallization temperature of mixtures of pyrene and LLDPE plotted on the calculated equilibrium phase diagram. (d) Crystallization temperature of mixtures of HMB and LLDPE plotted on the calculated equilibrium phase diagram.

HMB are identical, L−L demixing is not expected. Neat HMB as received from Fisher Scientific exhibits two melting peaks, a major one at 167 °C and a minor one at 112 °C (Figure 2a); the minor peak is assumed to be caused by impurities and is ignored in the analysis.

Phase Separation by Crystallization. Analyses in the previous section are from solely a thermodynamic perspective and kinetic factors could be important if the cooling is fast and thermodynamic equilibrium is not maintained during crystallization. Under nonequilibrium cooling conditions, both composition and temperature distribution in each phase may not be uniform. In this regard, dynamic crystallization processes were investigated using DSC and optical microscopy. The difference in crystallization behavior between pure pyrene and pure HMB is shown in Figure 3. HMB nucleates easily and crystallizes with relatively little supercooling while pyrene requires significant supercooling for crystallization. The width of crystallization peak suggests that HMB crystallizes relatively slowly while pyrene crystallizes very quickly. These differences in crystallization kinetics may be intrinsic properties of the diluents or due to impurities functioning as nucleating agents; regardless, the kinetics are reproducible. The crystallization characteristics of each diluent directly affect the crystallization behavior of the mixtures of LLDPE with pyrene and HMB. The effect of the diluent identity on the phase separation process is emphasized in Figure 4 which shows data for HMB and pyrene samples with the same LLDPE volume fraction ($\phi_2 = 0.25$). It is evident from Figure 4a that the temperature at which pyrene crystallizes in the polymer solution is much lower than that of HMB (127 °C vs 159 °C). Also apparent in Figure 4a is that the width of the crystallization peak of pyrene for the pyrene/LLDPE mixture is significantly narrower than that of HMB for the HMB/LLDPE mixture. This indicates that the crystallization rate of pyrene in the pyrene/LLDPE mixture is much higher than that of HMB in the HMB/LLDPE mixture. Optical microscopy shows that the solidification of pyrene is characterized by dendritic growth with a much higher rate than that of HMB (Figure 4b). Solidification of pyrene can be explained by the general theory of dendritic solidification, which is characterized by a morphology resulting from the growth of long, thin spikes in specific crystallographic directions, with regular branches in other equivalent directions.[19] It is known that dendritic growth takes place when, and only when, the melt is supercooled, and the growth rate is determined by the supercooling (temperature difference between the actual temperature of the interface and the equilibrium temperature). Experimental results in the literature indicate that the advancing rate of the tip of a dendrite (v) is roughly proportional to the square of supercooling ($(\Delta T)^2$).[20] This is in agreement with our observation that pyrene, which crystallizes after significant supercooling, shows fast dendritic solidification while HMB, which crystallizes after a much lower degree of supercooling, shows slow nondendritic solidification.

The solid−liquid interface present during crystallization of diluents was further investigated by polarized optical microscopy as shown in Figure 5. Thin (~10 μm) samples of diluent/LLDPE (3/1, w/w) mixtures were quickly quenched from 200 to 20 °C so that the crystallization process would be kinetically trapped and could be observed. Figure 5a shows that HMB easily nucleates and that crystals of HMB grow in random orientation in the liquid phase. Both HMB crystals and LLDPE spherulites are seen in the liquid phase near the solid−liquid interface, indicating that both components crystallize independently in the same region. In contrast, pyrene shows dendritic growth and new crystals do not form in the liquid phase (Figure 5b).

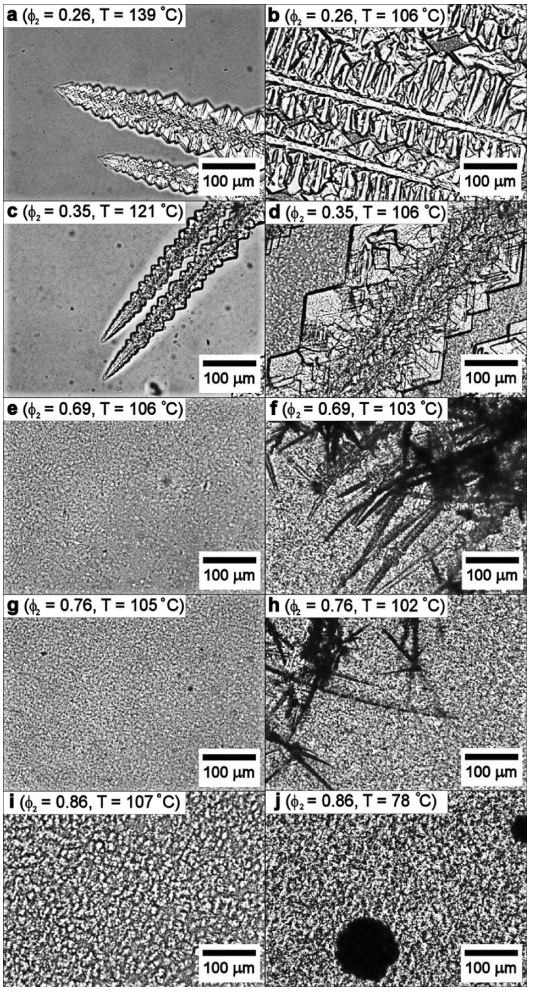

Figure 7. Optical microscopy images of pyrene/LLDPE mixtures. Samples were cooled from 200 to 30 °C at a 5 °C/min. ϕ_2 is the volume fraction of LLDPE.

Only LLDPE spherulites are seen in the liquid phase. Dendritic growth of pyrene is observed and crystallization proceeds into the highly supercooled liquid. The heat of crystallization (generated at the solid−liquid interface where crystallization takes place) causes the temperature of the S−L interface to be higher than that of the neighboring phases. Temperature gradients decreasing in both directions away from the S−L interface into both solid and liquid phases are present. Initially flat S−L interfaces tend to undergo fluctuation that is induced by thermal and/or concentration fields, if the crystallization is fast or is limited by diffusion. In these situations, any projection into the supercooled liquid experiences a lower temperature than the unperturbed interface, and crystallization of the projected tip is accelerated. Thus, a flat interface between a crystallizing solid and a supercooled liquid is inherently unstable and dendritic growth of crystals occurs.[19] Since the crystallization of pyrene takes place under highly supercooled conditions and the crystallization rate is high, a significant amount of heat due to crystallization is rapidly generated at the S−L interface, and the resulting temperature gradient leads to strong dendritic growth of pyrene crystals. Figure 5b also shows that the size of the LLDPE spherulites decreases as the distance from the interface increases. The concentration of LLDPE in the liquid phase is highest near the interface (due to the consumption of pyrene due to crystallization) and decreases with distance from the interface.

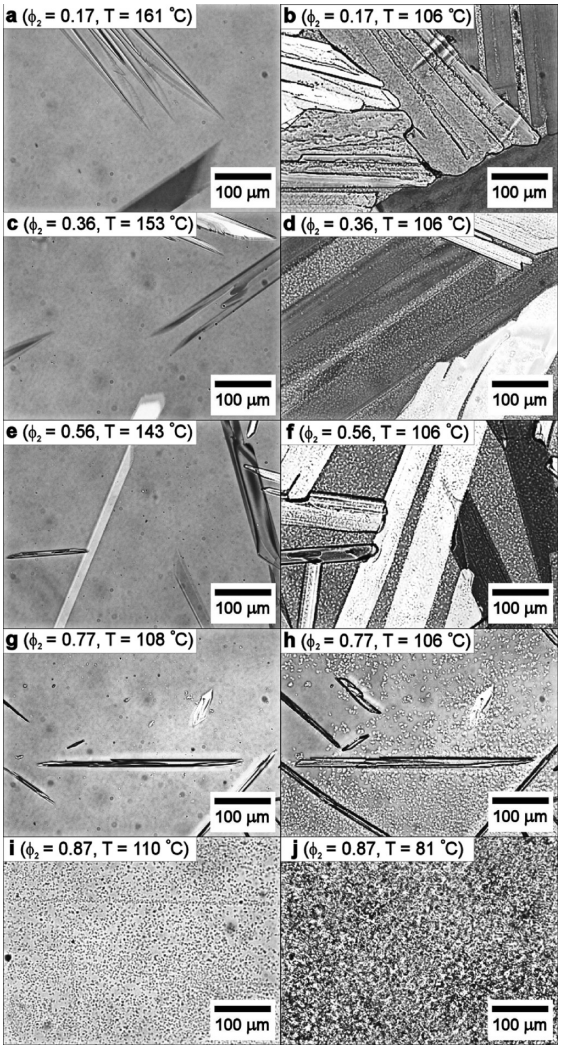

Figure 8. Optical microscopy images of HMB/LLDPE mixtures. Samples were cooled from 200 to 30 °C at a 5 °C/min. ϕ_2 is the volume fraction of LLDPE.

The resulting size distribution of LLDPE spherulites is likely due to this concentration gradient. We note that eutectic solidification in the liquid phase is not expected under these rapid cooling conditions because of the concentration and temperature inhomogeneities that exist in the liquid phase.

Samples with different composition show similar behavior. DSC thermograms in cooling runs and measured crystallization temperatures are shown in Figure 6. The gap between crystallization temperatures of pyrene and LLDPE decreases as the volume fraction of LLDPE increases (Figure 6a,c) until it reaches the eutectic composition, after which only one crystallization temperature is observed. A similar trend is observed for the crystallization of HMB/LLDPE mixtures (Figure 6b,d). The gaps between the two crystallization peaks of the HMB/LLDPE mixtures are larger than those of pyrene/LLDPE mixtures at similar composition levels.

The crystal growth of diluents in samples of different composition as observed by optical microscopy is shown in Figures 7 and 8. Dendritic solidification is clearly seen for pyrene/LLDPE mixtures when the initial composition is pyrene-rich (Figure 7a−d). Dendrite arms grow in specific crystallographic directions, these being uniquely determined by the crystal structure of pyrene.[20] The reason for this

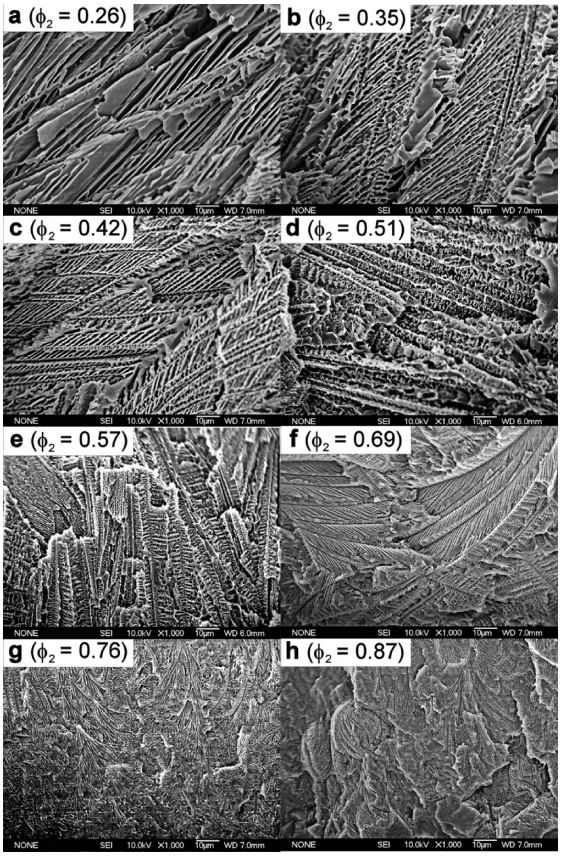

Figure 9. SEM micrographs showing the morphology of fractured cross sections of pyrene/LLDPE mixtures after extraction of pyrene. ϕ_2 represents the volume fraction of LLDPE.

observation is not fully understood, but the dendrite direction has been interpreted simply as the fastest growing direction of the crystal structure of pyrene.[19] As the LLDPE content increases and the composition of the mixture approaches the eutectic composition, both components tend to crystallize competitively. Since the eutectic composition is located far from the 50/50 (pyrene/LLDPE) composition, irregular or needlelike solidification is observed in eutectic solidification (Figure 7e−h).[20] Because of their different crystal structure and size, both components apparently crystallize independently. Figure 7e−h shows that the phase separation is initiated by LLDPE crystallization promptly followed by pyrene crystallization so that both components crystallize at the same time (eutectic solidification), which is observed as one crystallization peak in DSC cooling experiments (Figure 6a). In the case of HMB/LLDPE mixtures, dendritic solidification of HMB is less obvious due to the small supercooling for crystallization. Phase separation is initiated by the crystallization of HMB unless the initial LLDPE content in the mixture is greater than the eutectic composition (Figure 8a−f). In this case, platelike or needlelike crystals of HMB with no higher order branches are observed. When the initial composition is close to the eutectic composition, both components crystallize competitively but independent of each other (Figure 8g,h). If the LLDPE content in the mixture is higher than the eutectic composition, phase separation is initiated by LLDPE; HMB crystallization is not observed in these cases (Figure 8i,j). These observations indicate that the morphology as determined by the phase separation process strongly depends on the identity of the crystallizable diluents as well as the initial composition of the mixtures.

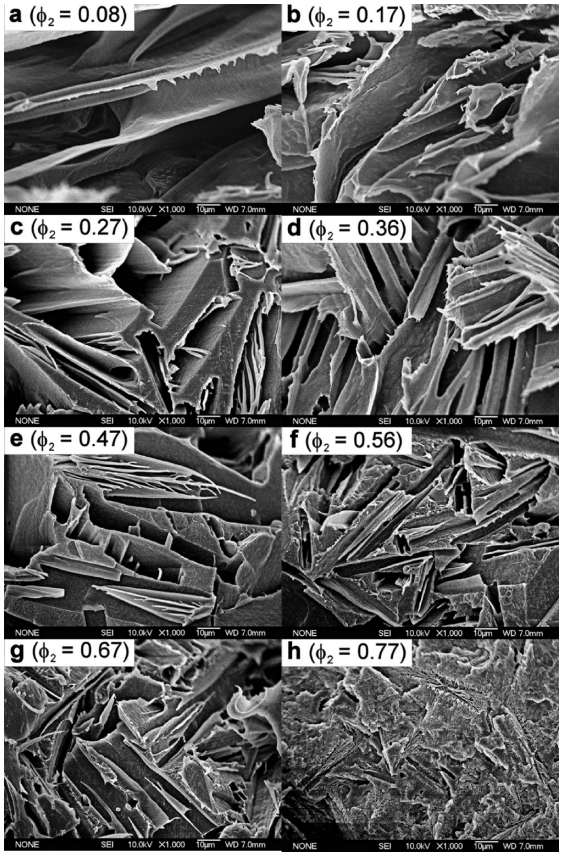

Figure 10. SEM micrographs showing the morphology of fractured cross sections of HMB/LLDPE mixtures after extraction of HMB. ϕ_2 represents the volume fraction of LLDPE.

Morphology. Figure 9 shows SEM micrographs of fractured cross sections taken from mixtures of LLDPE and pyrene after extraction of pyrene. Porous structures inside of each sample were formed by the crystallization of pyrene; the pores were occupied by pyrene crystals prior to extraction. Phase separation is triggered by the crystallization of pyrene for pyrene-rich samples as shown in the DSC and optical microscopy experiments (Figures 6 and 7), and the resulting porous morphology reflects the crystal growth characteristics of pyrene. The resulting porous material shows locally aligned porous layers stacked together (Figure 9a). As observed by optical microscopy, pyrene crystals grow in relative preferential directions. As the amount of pyrene in the sample decreases, less pyrene is available for crystal growth, and the resulting porous structure becomes smaller in size and each porous layer is not vacant but is filled with smaller pores (Figure 9b,c). Preferential direction of crystal growth is still apparent. When pyrene concentration is further decreased so that the LLDPE volume fraction in the sample is 0.51 and 0.57, pore size becomes even smaller and the internal structure inside each porous layer becomes more complex (Figure 9d,e). At LLDPE volume fractions of 0.69 and 0.76, the layered structure of pores is mostly lost (Figure 9f,g). In this composition regime, the majority of pyrene crystallizes at the same temperature as LLDPE (Figure 6a,c). Pores become so small that they can hardly be seen at the micrometer scale, and the morphology reflects the precipitation pattern of the pyrene crystals visualized in optical microscopy experiments (Figure 7f,h).

Porous structures from mixtures of LLDPE and HMB are very different from those of pyrene/LLDPE mixtures as shown in Figure 10. HMB produces platelike pores much larger in size than those of pyrene at similar LLDPE volume fractions. The local direction of HMB crystal growth is less aligned. Porous structures directed by HMB crystallization are observed when the LLDPE volume fraction is below 0.67 (Figure 10a−g). HMB crystallizes before LLDPE upon cooling in these samples as confirmed by DSC experiments (Figure 6b,d). With the volume fraction of LLDPE of 0.77 (close to the eutectic composition), platelike porous structures are no longer seen. HMB and LLDPE crystallize at the same temperature in these samples as observed by DSC (Figure 6b,d). The morphology as observed by SEM indicates that the microporous structure can be controlled by the identity of the crystallizable diluents as well as the composition of the mixtures.

Conclusions

Locally anisotropic porous materials have been prepared using high melting temperature diluents and a semicrystalline polymer. Diluents were selected that form homogeneous mixtures with the polymer at elevated temperature but undergo phase separation upon cooling. Since the crystallization temperatures of the selected diluents are higher than that of the polymer, phase separation is triggered by the crystallization of the diluent in the polymer solution, providing that there is a sufficient amount of diluent in the mixture. The crystallization of diluent continues until eutectic solidification begins, after which the structure is fixed. Porous materials are obtained by extracting the diluent crystals from the solidified samples. Phase separation can also be triggered by the crystallization of the polymer if the initial composition of the mixture is highly polymer-rich (higher than eutectic composition). In this case, samples do not show visible porous structures at micrometer scales. Since the porous structures obtained from diluent-rich samples are determined by the crystal growth characteristics of the diluent, the final shape and size of the pores depend strongly on the type of diluent as well as the composition of the mixtures. Hexamethylbenzene (HMB) forms relatively large, platelike pores while pyrene produces relatively small, better aligned layers of pores. Crystallization of pyrene requires much greater supercooling than that of HMB, leading to dendritic solidification which is characterized by a morphology resulting from the formation of slender spikes in specific crystallographic directions with regular branches in other equivalent directions. HMB, on the other hand, crystallizes at small supercooling and does not develop any noticeable dendritic structure. This result demonstrates that the microstructure of the porous polymeric materials can be controlled by the choice of the high melting diluents as well as the composition of the polymer solutions.

Acknowledgment. We thank the NSF-sponsored Centers for Hierarchical Manufacturing (CMMI-0531171) and Materials Research Science and Engineering (DMR-0213695) at the University of Massachusetts for support.

References and Notes

(1) Lloyd, D. R. *J. Membr. Sci.* **1990**, *52*, 239–261.
(2) Matsuyama, H.; Teramoto, M.; Kudari, S.; Kitamura, Y. *J. Appl. Polym. Sci.* **2001**, *82*, 169–177.
(3) Kim, W. K.; Char, K.; Kim, C. K. *J. Polym. Sci., Part B: Polym. Phys.* **2000**, *38*, 3042–3052.
(4) Matsuyama, H.; Yuasa, M.; Kitamura, Y.; Teramoto, M.; Lloyd, D. R. *J. Membr. Sci.* **2000**, *179*, 91–100.
(5) Matsuyama, H.; Berghmans, S.; Batarseh, M. T.; Lloyd, D. R. *J. Membr. Sci.* **1998**, *142*, 27–42.
(6) Narkis, M.; Siegmann, A.; Puterman, M.; DiBenedetto, A. T. *J. Polym. Sci., Polym. Phys. Ed.* **1979**, *17*, 225–234.
(7) Smith, P.; Pennings, A. J. *J. Polym. Sci., Polym. Phys. Ed.* **1977**, *15*, 523–540.

(8) Smith, P.; Pennings, A. J. *Polymer* **1974**, *15*, 413–419.
(9) Alwattari, A. A.; Lloyd, D. R. *J. Membr. Sci.* **1991**, *64*, 55–68.
(10) Glusker, J. P.; Lewis, M.; Rossi, M. *Crystal Structure Analysis for Chemists and Biologists*; VCH: New York, 1994.
(11) Kitaigorodsky, A. I. *Molecular Crystals and Molecules*; Academic Press: New York, 1973.
(12) Brandrup, J.; Immergut, E. H.; Grulke, E. A. *Polymer Handbook*, 4th ed.; Wiley: New York, 1999.
(13) Dobbs, J. M.; Wong, J. M.; Johnston, K. P. *J. Chem. Eng. Data* **1986**, *31*, 303–308.
(14) Poerschmann, J.; Kopinke, F. D. *Environ. Sci. Technol.* **2001**, *35*, 1142–1148.
(15) Barton, A. F. M. *CRC Handbook of Polymer-Liquid Interaction Parameters and Solubility Parameters*; CRC Press: Boca Raton, FL, 1990.
(16) Flory, P. J. *Principles of Polymer Chemistry*; Cornell University Press: Ithaca, NY, 1953.
(17) Burghardt, W. R. *Macromolecules* **1989**, *22*, 2482–2486.
(18) Mandelkern, L. *Crystallization of Polymers*; Cambridge University Press: Cambridge, 2002.
(19) Chadwick, G. A. *Metallography of Phase Transformations*; Butterworths: London, 1974.
(20) Chalmers, B. *Principles of Solidification*; John Wiley and Sons: New York, 1964.